Energy & Environmental Science

Accepted Manuscript

ROYAL SOCIETY OF CHEMISTRY

www.rsc.org/ees

Journal Name

ARTICLE

A novel solid-state Li-O_2 battery with an integrated electrolyte and cathode structure

Received 00th January 20xx,
Accepted 00th January 20xx

DOI: 10.1039/x0xx00000x

www.rsc.org/

X. B. Zhu, T. S. Zhao,* Z. H. Wei, P. Tan and G. Zhao

A high internal resistance and limited triple-phase boundaries are two critical issues that limit the performance of conventional solid-state Li-O_2 batteries. In this work, we propose and fabricate a novel solid-state Li-O_2 battery with an integrated electrolyte and cathode structure. This design allows a thin electrolyte layer (about 10% of that in conventional batteries) and a highly porous cathode (78% in porosity), both of which contribute to a significant reduction in the internal resistance, while increasing triple-phase boundaries. As a result, the battery outputs a discharge capacity as high as 14,200 mA h g^{-1}_{carbon} at 0.15 mA cm^{-2}, and can sustain 100 cycles at a fixed capacity of 1,000 mA h g^{-1}_{carbon}. The novel integrated electrolyte and cathode structure represents a significant step toward the advancement of Li-O_2 batteries.

Introduction

Li-O_2 batteries can theoretically release an energy density of 11,680 W h kg^{-1}_{Li} by integrating the lightest metal lithium with readily available ambient oxygen. This value is comparable to that of gasoline (13,000 W h kg^{-1}), and possesses the potential to replace conventional unrenewable sources of energy.[1-3] Even based on the consideration of the entire battery system, the capacity of ~1,000 W h kg^{-1} is still several times higher than that of Li-ion batteries.[4] Thus, Li-O_2 batteries have been attracting increasing attention as a possible green alternative to current lithium-ion batteries for electric vehicles.[2,3] Despite the promising performance, several issues still exist in practical Li-O_2 battery operation. One major issue is associated with the use of liquid electrolytes, which causes several problems including evaporation, leakage, flammability, low oxygen solubility and diffusion, and chemical and/or electrochemical instabilities.[5-7] These issues can be alleviated by the use of a solid-state electrolyte. In addition, the solid-state electrolyte layer can shield the Li anode from oxygen, CO_2 and moisture in the air, significantly improving the stability of Li-O_2 batteries for long-term operation. Meanwhile, solid-state electrolyte can also serve as a physical barrier to avoid short circuiting caused by Li dendrites during long-term operation.[8-10] In a recent review paper summarizing lithium-ion conducting membranes for lithium-ion or Li-O_2 batteries were classified in three categories,[2,7,10] including polymer and polymer/ceramic, single-crystal silicon membranes, and non-oxide and oxide based inorganic materials. Each type of membrane exhibits notable strengths and weaknesses. For example, the most critical problem for non-oxide based inorganic materials (LiM_x, M = N, I, S, OH, *etc.*), is deliquescence in ambient air and aqueous electrolytes. Oxide based inorganic materials (Perovskite-type, Garnet-type, γ-Li_3PO_4-type and NASICON-type) also present various concerns, they are not entirely debilitating.

Lithium aluminium titanium phosphate (LATP) ceramics with NASICON structure have attracted much attention due to an extremely high Li-ion conductivity of 7×10^{-4} S cm^{-1}, including bulk conductivity of 3×10^{-3} S cm^{-1} and grain boundary conductivity of 9×10^{-4} S cm^{-1},[8] they have been widely employed as the electrolyte material for all-solid-sate lithium-ion batteries.[11-13] The LATP was initially developed to serve as a separator and Li protector for hybrid electrolytes in Li-O_2 batteries.[14-16] In 2011 a Li-O_2 battery with a configuration of Li metal | organic electrolyte | LATP | carbon cathode was examined by Zhou *et al.*, which demonstrated a discharge capacity of 950 mA h g^{-1}_{carbon} at a current density of 0.1 A g^{-1}_{carbon} and a cutoff voltage of 2.0 V.[17] In this battery, the solid-state carbon cathode was directly connected with the LATP electrolyte surface, eliminating the use of liquid electrolytes at the cathode side, but the active sites were restricted to the interface between the solid-state electrolyte and the cathode, resulting in a very limited triple-phase boundary (TPB). They further modified the cathode structure with a mixture of LATP and carbon powders, using connected LATP particles to provide Li^+ pathways inside the cathode.[18] However, the two types of particles are randomly distributed, which is not ideal in forming a continuous pathway for electrons and Li^+, and leads to particle isolation (material waste and activity loss). Huang *et al.* used Pt modified carbon nanotubes filled with ionic liquid electrolyte as the cathode, creating a Li^+ pathway inside the cathode, and thereby achieving a discharge capacity as high as 9,092 mA h g^{-1}_{carbon}.[19] This result indicates that the expanded reaction sites play an indispensable role in enhancing battery performance, and at the same time, demonstrates the fact that solid-state Li-O_2 batteries exhibit very limited TPB. In

Department of Mechanical and Aerospace Engineering, The Hong Kong University of Science and Technology, Clear Water Bay, Kowloon, Hong Kong SAR, China. E-mail: metzhao@ust.hk (T.S. Zhao)

conclusion, there are at least two significant technical challenges for the development of solid-state Li-O_2 batteries: (i) high internal resistance. In conventional solid-state Li-O_2 batteries, the solid-state electrolytes exist independently, demanding a need to set its thickness (150~800 μm) to meet the required mechanical properties for practical application. Additionally, Li^+ conductivities for existing solid-state electrolyte materials are reported to be at only a tenth to a hundredth of the conductivities of liquid electrolytes, suggesting that the electrolyte layer causes severe ohmic loss;[1,20] (ii) limited TPBs. For conventional solid-state Li-O_2 batteries, TPBs are typically limited to the interfaces between the solid-state electrolyte and cathode,[21,22] which are much smaller in area than those of Li-O_2 batteries using liquid electrolytes where cathodes are completely saturated.

In this study, a novel battery configuration is proposed to address these issues, as schemed in Fig. 1, in which the key component is an integrated LATP pellet that is used as both the electrolyte and the porous cathode support. In this set-up, the electrolyte layer does not exist independently but is part of the entire system, alleviating the demand for mechanical strength. Thus, its thickness can be reduced from 600 μm to 36 μm to minimize ohmic loss. In contrast to conventional cathodes saturated with liquid electrolytes, in which low oxygen solubility and partial pressure were commonly considered to be the rate-limiting steps,[23-25] this novel cathode with a high porosity of 78% has the ability to provide broader cavities for active particle accommodation and solid products deposition, which creates more pathways for gaseous oxygen molecules transporting directly to active sites with much higher $P(O_2)$. Furthermore, due to the absence of liquid electrolytes at the cathode side, the problem of evaporation for an open system was eliminated. A nano-thin carbon layer was prepared onto the interior surface of the LATP scaffold via an impregnation process to serve as both electron conductors and catalysts of the cathode. As a result, the active sites or TPBs were expanded from a limited interface to the entire cathode with the help of LATP networks to provide criss-cross Li^+ pathways. A decline in the electrochemical polarization is expected due to the rich contact areas between carbon and LATP. Our results provide evidence of enhanced performance in the discharge capacity, rate performance and cycle life for the novel Li-O_2 batteries.

Experimental

Integrated LATP pellets preparation

Electrochemical reactions within Li-O_2 batteries depend heavily on the thickness of the LATP electrolyte layer. Electrolytes that are thin and dense are ideal. Meanwhile, a highly porous cathode for the process of impregnation will provide more storage and loading space with much richer input and output channels. The preparation of an ultra-thin and ultra-dense LATP membrane onto a highly porous LATP matrix is considered the biggest technical challenge since LATP materials suffer from two critical weaknesses: (i) extreme sensitivity to sintering temperature and duration, and (ii) prone to micro-crack formation due to high thermal expansion anisotropy of the crystal lattice.[1,26]

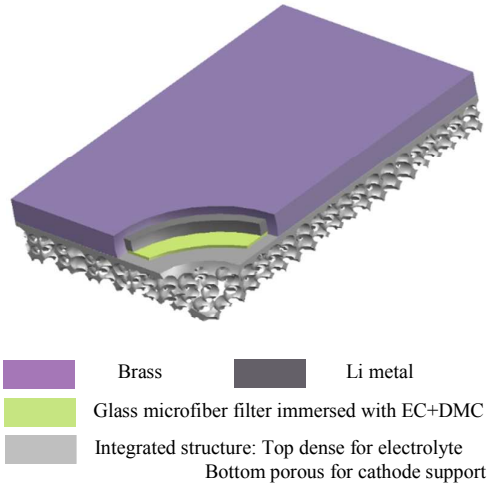

Fig. 1 Schematic illustration of the novel Li-O_2 battery with an integrated solid-state electrolyte and cathode structure.

In this study, $Li_{1.3}Al_{0.3}Ti_{1.7}(PO_4)_3$ (LATP) raw powders were prepared via two different methods, including solid phase reaction and sol-gel. The reagents used in this paragraph are all from Sigma-aldrich, Germany. For solid phase reaction, Li_2CO_3, Al_2O_3, TiO_2, and $(NH_4)H_2PO_4$ were ball-milled in ethanol for 30 h, dried at room temperature, and heated at 900 °C for 5 h. 20% excess lithium was included in the mixture to avoid the deficiency of lithium in the prepared specimens. For sol-gel, a precursor sol was prepared from $LiNO_3$, $Al(NO_3)_3{\cdot}9H_2O$, $Ti\{OCH(CH_3)_2\}_4$, $(NH_4)H_2PO_4$, HNO_3 and H_2O_2, which was finally heated at 800 °C for 5 h after pre-heating at 100 °C for 24 h. 10% excess lithium was included in the sol to avoid the deficiency of lithium in the prepared specimens.

To prepare the porous cathode support, LATP powders (prepared by sol-gel) and starch (as pore former, the particle dimensions of starch are shown in Fig. S1, Sigma-aldrich, Germany) were thoroughly mixed in a weight ratio of 6 : 5, uniaxially pressed into pellets under 200 M Pa, and sintered at 850 °C for 15 h to enhance its mechanical strength. The LATP membrane was then coated onto one surface of pre-sintered LATP pellets by a slurry spin-coating technique (3,000 rmp) and finally sintered at 1,000 °C for 5 h to form an integrated structure. There is no interface between the electrolyte and cathode support since the same materials are used, eliminating the potential barrier at the conventional interface between electrolyte and electrode and allowing faster transport of Li^+. The slurry for spin-coating was prepared from two kinds of LATP raw powders (sol-gel and solid phase reaction) mixed with terpilenol (Kermel, Tianjin, China), ethyl cellulose (Kermel, Tianjin, China) and polyvinyl pyrrolidone (PVP, Sigma-aldrich, Germany) at a weight ratio of 8 : 10 : 15 : 1 : 0.08, which was ball-milled for 24 h before use. The weight ratio of the two kinds of powders was calculated by the *Alfred*

Equation based on the results of particle size distribution. Since sintering is considered problematic for LATP materials,[1,26] as aforementioned, the use of mixed powders increases their apparent densities and improves their sintering properties, while the introduction of buffer agents (ethyl cellulose and PVP) modifies the sedimentation speed of suspension.

Carbon nanoparticles coated LATP cathode preparation

Sucrose (Sigma-aldrich, China) was dissolved into deionized water to form a precursor solution at 10 wt.%. The solution was subsequently impregnated onto the LATP scaffold (Fig. S2a) and heated at 150 °C for 30 min. (this impregnating-heating cycle was repeated 3 times). One-face impregnated LATP bilayers were fired at 650 °C for 3 h in pure Ar to obtain a uniform thin carbon coating of 2 or 3 mg cm^{-2} (projected area). It was named as a monolayer carbon coated LATP cathode, as shown in Fig. S2b. In this study, the carbon loading in the cathode was quantified by the volume of the infiltrated solution, which was controlled by a micro-syringe. A correlation between the volume of the solution and the mass after the thermal decomposition was obtained before loading carbon to the cathode.

Bilayer carbon coated LATP cathode preparation

Two kinds of bilayer carbon coated LATP cathode have been proposed and prepared successfully in this study. One is carbon fiber and carbon nanoparticles coated LATP cathode (Fig. S2c), the other is mesoporous carbon and carbon nanoparticles coated LATP cathode (Fig. S2d). For the first one, a carbon nanoparticles coated LATP cathode (Fig. S2b) was impregnated with 0.05 M $Ni(NO_3)_2$ aqueous solution. After dried at 150 °C for 30 min., the impregnated cathode was reduced at 650 °C for 10 min. with 5% H_2 + Ar and then exposed to the ethanol vapour for 10 min. to deposit carbon fibers onto the surface of carbon nanoparticles, achieving a bilayer carbon coated LATP cathode as shown in Fig. S2c. For the other one, mesoporous carbon is prepared by using Pluronic F127 (Sigma-aldrich, Germany) as the template and the soluble resol as the carbon precursor. Resol was prepared by mixing 1.0 g of phenol and 0.2 g of NaOH (20 wt.%, Sigma-aldrich, Germany) and 1.7 g of formaldehyde solution (37 wt.%, Sigma-aldrich, Germany). The pH value of the mixture was adjusted to 7.0 and dried under vacuum condition. To prepare mesoporous carbon, a certain amount of triblock copolymer Pluronic F127 and resol were dissolved in ethanol to form a solution, which was evaporated at room temperature for 8 h, followed by heating at 100 °C for 24 h. The product was finally heated at 600 °C for 2 h in pure Ar with a heating rate of 1 °C $min.^{-1}$. The prepared mesoporous carbon was ball-milled for 50 h and dispersed into ethanol to form a suspension. The carbon nanoparticles coated LATP cathode (Fig. S2b) was then immersed in the suspension for 30 min. with the assistant of ultrasound to deposit the mesoporous carbon into porous cathode, achieving another kind of bilayer carbon coated LATP cathode as shown in Fig. S2d.

Battery assembly and test

As-prepared LATP pellets, integration of thin electrolyte and the carbon coated porous cathode were transported into an Ar-filled glove box system (Etelux, Lab 2000) with oxygen and water contents below 1 ppm. The schematic diagram of the Li-O_2 battery is shown in Fig. 1. At the anode side, Li metal was sandwiched between a brass lid and a dense LATP electrolyte, and was sealed with glue (WD1001, Shanghai Kangda New Materials Company, China). Brass was closely connected with Li and hence used as the current collector of the anode. A glass microfiber filter (Whatman, Cat. No. 1822-047) immersed with commercial electrolyte (EC : DMC = 1 : 3, Guangzhou Tianci Technology LTD. Co., China) was used to prevent the reaction between Li metal and LATP electrolyte[3,22] and connected to the Li^+ transport pathway. The liquid electrolytes were sealed into the compartment between the Li metal and LATP electrolyte in two steps. The liquid electrolyte, i.e., EC+DMC, was first impregnated into the porous glass microfiber filter. The glass microfiber filter was then sandwiched by Li metal and LATP electrolyte and sealed with glue (WD1001, Shanghai Kangda New Materials Company, China). In this work, a simple method of physical isolation is temporarily used to protect the LATP membrane from Li metal. In further work, a thin layer of $Li_7La_3Zr_2O_{12}$ should be considered for protecting the LATP surface. No reactions with lithium metal have been reported as of yet.[27,28] After assembly, batteries were examined at room temperature under pure O_2 or Ar. The galvanostatic charge and discharge tests for the Li-O_2 batteries were conducted on a battery test system (Neware, CT-3008 W) at different current densities (0.1~13 mA cm^{-2}) with a cutoff voltage of 2.0 V. The cycle performance was demonstrated with a cutoff capacity of 1,000 and 5,000 mA h g^{-1}_{carbon} at a constant current density of 0.15 mA cm^{-2}.

Characterization

The stability of the LATP electrolyte before and after battery testing over two months was measured with a Philips high resolution X-Ray Diffraction system (XRD, model PW1825) using a Cu Kα source operating at 40 k eV. The porosity and pore distribution of the pristine cathode were investigated with a mercury intrusion porosimetry (MIP, Micromeritics Instrument Corporation AutoPore IV 9500, USA). The micrographs for a monolayer carbon impregnated porous cathode at different charge or discharge depths were generated with scanning electron microscopy (SEM) using JEOL-6300, JEOL-6390 and JEOL-6700F scanning microscopes. XRD, Fourier transform infrared (ATR-FTIR, Vertex 70 Hyperion 1000) and Micro-Raman (In Via, Renishaw) spectroscopy measurements for the above cathodes were also conducted to identify the discharge products.

Results and discussion

Morphology of the integrated structure

As presented in Fig. 2a and b, the top dense layer served as the electrolyte (36 μm thick, 97% dense) while the bottom porous layer served as the cathode support. According to the MIP

results, for the cathode, the median pore diameter (Volume) is 6.9 μm, the median pore diameter (Area) is 1.5 μm, the average pore diameter (4V/A) is 2.9 μm, and the porosity is 78%. Since both the electrolyte and the cathode support were prepared using the same LATP material, the two layers were seamlessly connected without interfacial resistance. In contrast, conventional solid-state cathodes with a distinct physical interface causes inevitable ohmic and polarization losses.[19] Fig. 2c shows one pore in the porous cathode support and displays clear LATP grain boundaries, which were blurred after coating with 2 mg cm^{-2} carbon nanoparticles, as shown in Fig. 2d. The uniform carbon coating has a thickness of ~10 nm (insert), which served as both electron conductor and catalyst for the electrochemical reaction in the impregnated cathode.

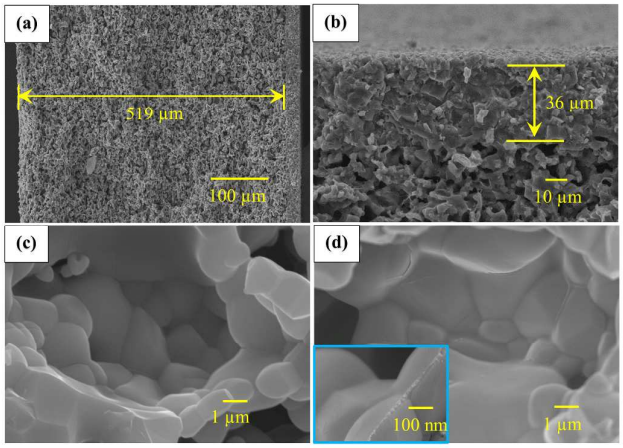

Fig. 2 The SEM images for (a), (b) integrated structure, (c) one pore in porous cathode support before carbon loading, and (d) one pore in porous cathode support after carbon coating. The insert shows the thickness of carbon layer on LATP scaffold prepared by an impregnation and pyrolysis process.

Discharge/charge performance and product analysis

The discharge and charge curves of the Li-O_2 battery with an integration of the cathode and electrolyte, at a constant current density of 0.15 mA cm^{-2}, are shown in Fig. 3a. The battery delivered a discharge capacity of 14,200 mA h g^{-1}_{carbon}, with a voltage plateau of 2.65 V (*vs.* Li^+/Li). Compared with a Li-O_2 battery with a configuration of Li | organic electrolyte | LATP | carbon cathode which exhibits a discharge capacity of 950 mA h g^{-1}_{carbon},[17] the adoption of this integrated structure enabled a 15-fold increase in battery capacity. Moreover, the achieved capacity is comparable to that of liquid electrolytes based Li-O_2 batteries.[25,29,30] The high capacity is attributed to extended TPBs, from the interface to the entire electrode. Only one voltage plateau of about 3.75 V was presented in the recharge curve, and the terminal voltage was 4.17 V, indicating that it is possible to fully recharge the battery. In addition, the voltage plateau is lower than that of various liquid electrolyte based Li-O_2 batteries, especially at the terminal stage,[10,31] suggesting an improved energy efficiency.

It is generally understood that NASICON-type materials have been used as electrodes for Li-ion batteries[32] and Na-ion batteries.[33] This is due to the inductive effect of polyanions $(PO_4)^{3-}$ and $Ti^{4+} \rightarrow Ti^{3+}$, which displays a flat operating potential and undergoes a two-phase reaction mechanism, as follows:[34]

$$Li_{1.3}Al_{0.3}Ti^{4+}_{1.7}(PO_4)_3 + 1.7Li^+ + 1.7e^- \leftrightarrow Li_3Al_{0.3}Ti^{3+}_{1.7}(PO_4)_3 \quad (1)$$

Eq. 1 indicates that the discharge/charge capacity of the LATP based Li-O_2 battery will be affected by the electrochemical Li-insertion/extraction capacity of LATP itself. A similar Li-O_2 battery was thus tested with pure Ar at a current density of 0.15 mA cm^{-2} and a cutoff voltage of 2.0 V. Without oxygen, the carbon coating over the LATP surface no longer served as a catalyst but instead became an electron pathway. Furthermore, owing to the poor electrical conductivity of LATP, carbon coating is necessary to maximize the use of the inner surface of porous LATP support during the Li-insertion process. As shown in Fig. 3b, the same battery did not display a distinct plateau during discharge and charge processes under pure Ar. Instead, the discharge voltage decreased almost linearly from 2.39 V to 2.0 V (*vs.* Li^+/Li) with increasing Li-insertion capacity. The capacity for Li-insertion corresponds to almost 35 mA h g^{-1}_{LATP} (0.5 moles of Li), which was calculated based off of the mass of the LATP support (47 mg cm^{-2}). The observed values are close to 30% of the theoretical capacity of 118 mA h g^{-1}_{LATP} for 1.7 moles of Li. A 70% loss is observed and is attributed to the porous structure of the solid-state cathode, in which only a small part of LATP grains close to the pore wall has the ability to insert or extract Li-ion. In the subsequent charge process, the charge voltage reached 4.52 V at the terminal stage (the same discharge capacity), and continuously increased to 5.0 V when being further overcharged. As illustrated in Fig. 3b, the potential for Li-insertion is apparently lower than that of Li→LiO_x. Moreover, there is a distinct voltage plateau of 2.65 V when discharging under pure O_2. In contrast, the potential decreased linearly from 2.39 V to 2.0 V under pure Ar, making it easy to differentiate between the Li-O_2 mechanism and Li-insertion mechanism. However, we are still unsure whether Li-insertion/extraction reactions occur under real operating conditions of Li-O_2 battery. It is estimated that the discharge capacity (35 mA h g^{-1}_{LATP}) accounts for only 5.8% of the whole discharge capacity (600 mA h g^{-1}_{LATP} = 14,200 mA h g^{-1}_{carbon} = 576 mA h $g^{-1}_{cathode}$ = 539 mA h $cm^{-3}_{cathode}$) of the battery with pure O_2 at a constant current density of 0.15 mA cm^{-2}, meaning that the capacity is predominately from the Li-O_2 mechanism, instead of the Li-insertion mechanism.

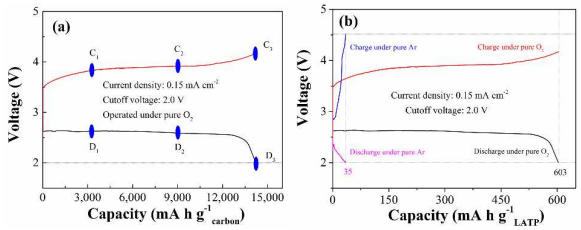

Fig. 3 Discharge/charge performances for the Li-O_2 battery with carbon loading of 2 mg cm^{-2} operated with (a) pure O_2 or (b) pure Ar at a constant current density of 0.15 mA cm^{-2} and a cutoff voltage of 2.0 V. When operating with pure O_2, similar batteries were stopped at different depths of discharge (D_1, D_2, D_3) and recharge (C_1, C_2, C_3) processes and then conducted SEM characterization. In (a) the discharge capacity density of the battery was calculated by the mass of carbon to compare with the results in the literature, while in (b) the discharge capacity densities were calculated by the mass of LATP (47 mg cm^{-2}) to confirm how much is the capacity contribution of LATP.

In order to visually understand the evolution of the discharge products during the discharge and charge processes under pure O_2, the cathodes at different discharge and charge stages (corresponding to six points in discharge/charge curves in Fig. 3 D_1, D_2, D_3 and C_1, C_2, C_3) were observed by SEM, as presented in Fig. 4. At a discharge capacity of 3,000 mA h g^{-1}_{carbon} (D_1), spherical particles with particle sizes on the scale of dozens of nanometers were observed over the carbon surface, which are much smaller than those in liquid electrolyte based Li-O_2 batteries and more favourable for recharging.[35-37] With an increase of the discharge depth comes an increase of particles which form a connected, layer-like morphology, as shown in Fig. 4c. At this condition, the pathway for gaseous oxygen to active sites is becoming clogged, causing a "sudden death" of the discharge process. For the following charge process, the number of particles gradually decreased with an increasing charge capacity, as shown in Fig. 4d and e. At the terminal of charge process, the nanoparticles were decomposed completely, as shown in Fig. 4f, indicating good reversibility, which is consistent with the discharge and charge curves in Fig. 3.

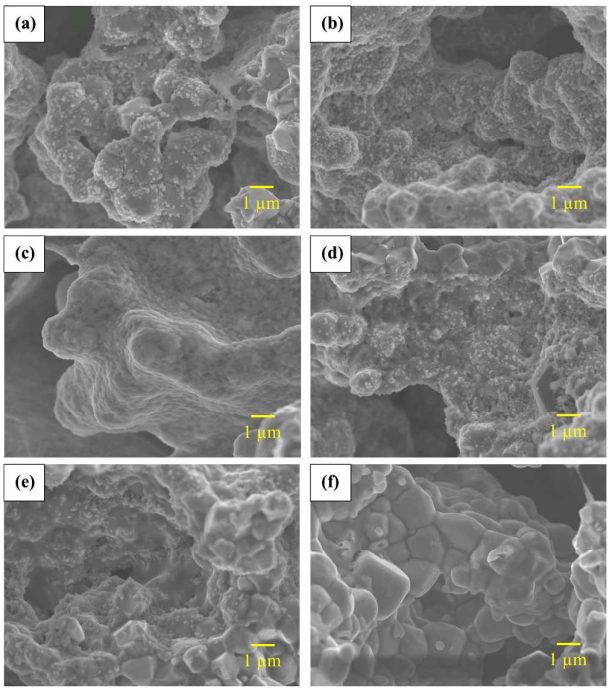

Fig. 4 The SEM images for the formation and decomposition of products inside the novel solid-state cathodes with carbon loading of 2 mg cm^{-2} during discharge and charge processes, (a) corresponding to D_1 in Fig. 3, (b) corresponding to D_2, (c) corresponding to D_3, (d) corresponding to C_1, (e) corresponding to C_2, and (f) corresponding to C_3.

After discharge, XRD was used to analyse the component of discharge products and confirm the stability of LATP electrolyte and cathode support, as shown in Fig. 5a. The peaks of LATP material before and after testing for about 2 months showed good consistency, demonstrating its chemical stability. Due to the strong intensity of the LATP, however, peaks corresponding to discharge products were difficult to detect. It is also because of the high porous cathode that allows the products to deposit onto its interior surface where X-ray is blocked. The peaks corresponding to carbon in the impregnated cathode were also not extremely obvious, but the effect of carbon coating on the intensity of LATP peaks could not be neglected, implying that there was formation of amorphous carbon after the heat treatment of sucrose solution at 650 ºC. In addition, the Raman technique was employed, as shown in Fig. 5b. Five peaks appeared corresponding to the impregnated cathodes after a full discharge. The existence of amorphous carbon was confirmed with two main signatures, a peak located around 1,590 cm^{-1} known as the graphitic (G peak, internal phenyl ring stretch) and 1,330 cm^{-1} from disordered graphitic islands (D peak).[38] However, it is difficult to prove the existence of Li_2O_2 since an overlap in the peaks of Li_2O_2 and LATP was observed at 789 cm^{-1}. Further evidence has been obtained from the Fourier transform infrared (FTIR) analysis and the results were illustrated in Fig. 5c. The corresponding peak of Li_2O_2 clearly appeared at 540 cm^{-1}, which is consistent with previously published results.[39] Moreover, the peak disappeared after being fully charged, suggesting the decomposition of Li_2O_2. Based on the porosity of the pristine cathode and the discharge capacity, the porosity occupied by Li_2O_2 after discharging to 2.0 V can be calculated to be 14%.

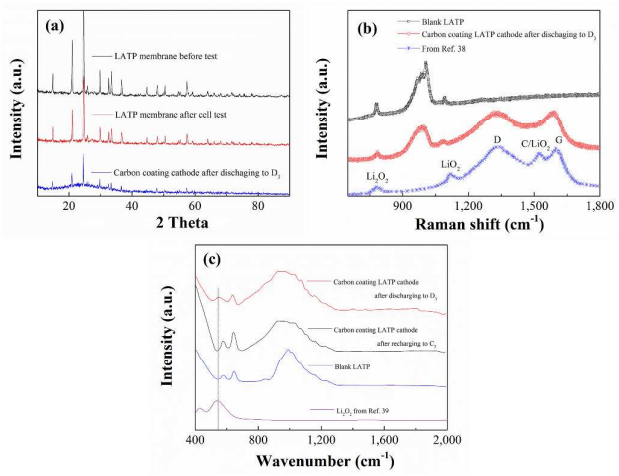

Fig. 5 (a) XRD analysis for a LATP membrane before and after cell test for about 2 months, and for a monolayer carbon coated cathode after full discharge to D_3. (b) Raman analysis for a blank LATP cathode support, and for a monolayer carbon coated cathode after full discharge to D_3. The peaks corresponding to Li_2O_2, LiO_2, C/LiO_2 and standard carbon D and G were marked in the bottom.[38] (c) FTIR demonstrates the formation and decomposition of product Li_2O_2 in a monolayer carbon

coated cathode after full discharge to D_3 and full recharge to C_3. Blank LATP and reference Li_2O_2 (from Ref. 39) spectra were used for comparison.

The discharge product for liquid electrolyte based Li-O_2 batteries has been widely investigated, and the toroidal microstructure corresponding to discharge product was proposed and confirmed by SEM and/or TEM.[40-42] It has been proposed that under galvanostatic discharge conditions, LiO_2 is an intermediate product formed at the initial stage, and gradually transforms into the ultimate product Li_2O_2 via a chemical and/or electrochemical process.[43-45] The originally formed LiO_2 can be dissolved into non-aqueous electrolytes, and deposited onto cathode surface as an insoluble Li_2O_2, gradually forming toroidal structure.[46-48] The aforementioned processes of dissolution and deposition are unlikely to occur in this novel solid-state cathode since liquid electrolyte was not used at the cathode side, thus lacking a transport medium. To understand the growth process of product particles over the solid-state cathode surface without a liquid Li^+ conductor, we propose a possible mechanism based on low-level Li^+ conductivity of product Li_2O_2.[49,50] According to the results of Siegel *et al.*,[51] the Li^+ conductivity of Li_2O_2 is 4×10^{-19} S cm^{-1} that is 10 times higher than the electrical conductivity of 5×10^{-20} S cm^{-1}. Viswanathan *et al.* have comprehensively investigated the thickness of a Li_2O_2 film to propagate electrons and maintain the discharge process for conventional non-aqueous Li-O_2 batteries, and given a restrict thickness of ~5 nm.[48] In conventional non-aqueous Li-O_2 batteries, the charge transport limitation arises from the fact that the electron from the conducting cathode must propagate through the product Li_2O_2 layer (covering electron conductor) to meet and react with Li^+ and O_2 from liquid electrolytes. In the present solid-state Li-O_2 battery, however, this limitation for charge transport is Li^+ but not the electron, which is needed to propagate through the product Li_2O_2 layer (covering Li^+ conductor) to meet with electron from carbon network and O_2 absorbed onto active sites (carbon surface). Through comparing the difference between electronic and Li^+ conductivities of product Li_2O_2, we can obtain the restrict thickness of the product layer in the novel solid-state cathode, ~50 nm (10 times increase). Based on that, a possible mechanism was proposed to reveal the deposition and growth process for Li_2O_2 onto the solid-state cathode. As schemed in Fig. 6, at first, the active sites (TPBs) are distributed in contact points between LATP backbone and carbon particles, such as A and B, where triple-phase (Li^+ from LATP, electron from carbon network, O_2 diffusion through cathode pores) can meet together. Product particles will initially form at A and B, and filled into the adjacent pin-pores in carbon layer, which has been demonstrated by the observation of a carbon coated cathode operated at 0.15 mA cm^{-2} with a cutoff capacity of 800 mA h g^{-1}_{carbon}. As shown in Fig. 7a, no obvious product particles were detected over carbon surface at the initial discharge stage (800 mA h g^{-1}_{carbon}), but some particles can be seen indistinctly through a nano-sized carbon coating, as shown in Fig. 7b, and the product particles can be further directly observed after peeling the carbon coating, as shown in Fig. 7c. This shows that the product growth is an inside-out process, *i.e.*, from the interface between LATP backbone and carbon coating to the interface between carbon coating and O_2. As displayed in Fig. 2d, the thickness of the carbon coating is ~10 nm, indicating a similar thickness of the filled Li_2O_2 layer, only 1/5 of the restrict thickness ~50 nm, therefore which can continuously transport Li^+ from LATP

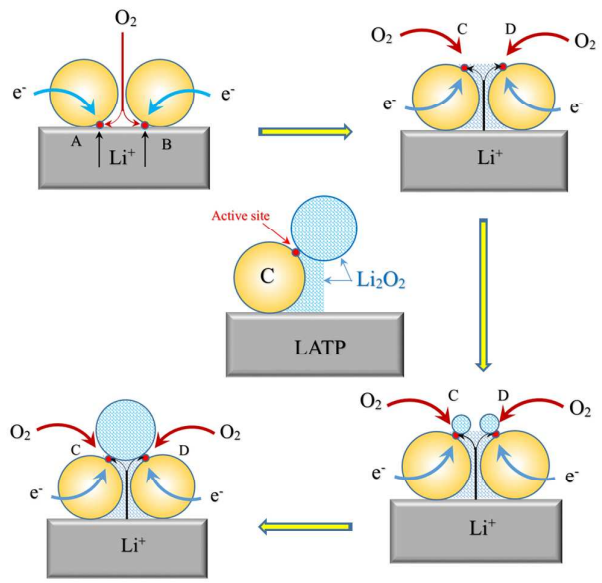

Fig. 6 Schematic diagram for product formation inside the monolayer carbon coated solid-state cathode during discharge process.

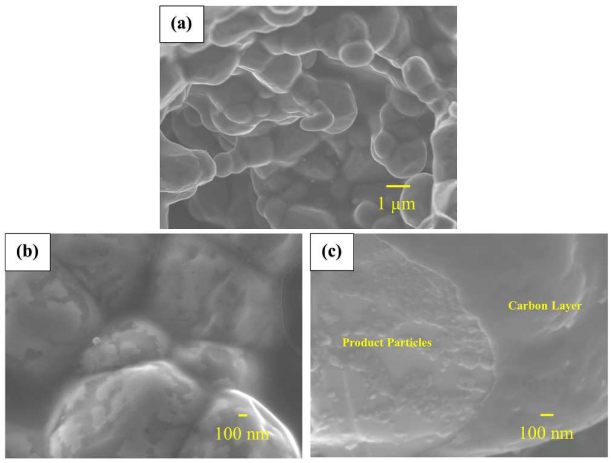

Fig. 7 The SEM images for discharge product in monolayer carbon coated cathode after operating under pure O_2, at a current density of 0.15 mA cm^{-2}, with a cutoff capacity of 800 mA h g^{-1}_{carbon}; (a) interior surface of a pore in the carbon coated cathode, (b) high magnification for (a), and (c) product particles between LATP scaffold and carbon coating layer.

backbone surface to carbon coating surface to maintain the discharge process. Secondly, as a result, the active sites were transported from A and B to C and D close to the outside surface of carbon coating. Thirdly, the product particles will

grow gradually at active sites C and D with increasing discharge depth. Fourthly, these particles connect with each other to create larger particles and to form a gas-tight layer over carbon coating at the end, as shown in Fig. 4c, thus resulting in a "sudden death" at the terminal stage of discharge (Fig. 3). At one contact point, Li_2O_2 particles can grow to a large sizes of up to 500 nm in diameter, which has been demonstrated by Zheng *et al.*.[52] They used Li-metal as a source of Li^+, a carbon nanotube as the electron pathway, and a Li_2O thin-layer over Li metal as the solid-state electrolyte. The discharge process were conducted under pure O_2, with the aid of the in situ technique in the ESEM to directly observe the growth process of Li_2O_2 at one contact point. More importantly, this experiment also confirmed the fact that products LiO_x can be utilized as the transport media for Li^+ during the charge and discharge processes.

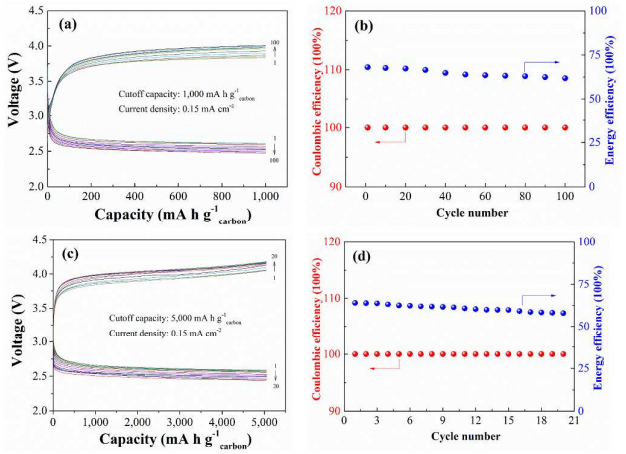

Fig. 8 (a), (c) Cycle performances and (b), (d) coulombic and energy efficiencies for the novel Li-O_2 battery with a monolayer carbon coated cathode operated under pure O_2 at a current density of 0.15 mA cm^{-2} with a limited capacity of (a), (b) 1,000 mA h g^{-1}_{carbon} and (c), (d) 5,000 mA h g^{-1}_{carbon}.

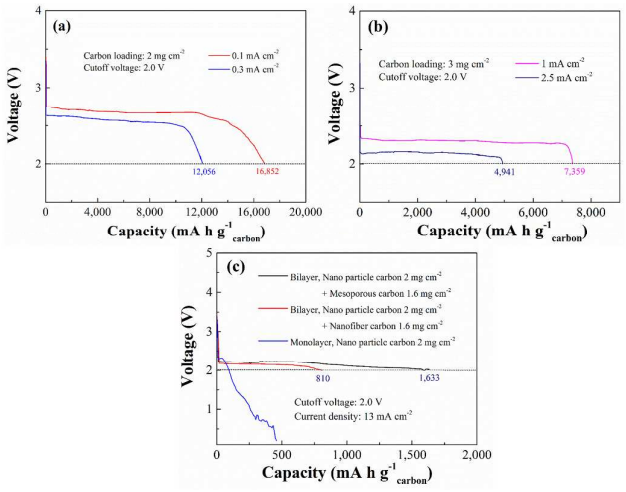

Fig. 9 Galvanostatic discharge curves (U vs capacity) for the novel Li-O_2 battery with a monolayer carbon coated cathode (a) at a current density of 0.1 and 0.3 mA cm^{-2} with a carbon loading of 2 mg cm^{-2}, and (b) at a current density of 1 and 2.5 mA cm^{-2} with a carbon loading of 3 mg cm^{-2}; (c) galvanostatic discharge curves for the novel Li-O_2 battery with a monolayer carbon coating cathode or a bilayer carbon coating cathode at the highest current density of 13 mA cm^{-2}. The monolayer carbon coating is packed by carbon nanoparticles, while the bilayer carbon coating composes of a top-layer of porous carbon nanofiber or mesoporous carbon and a bottom-layer of carbon nanoparticles.

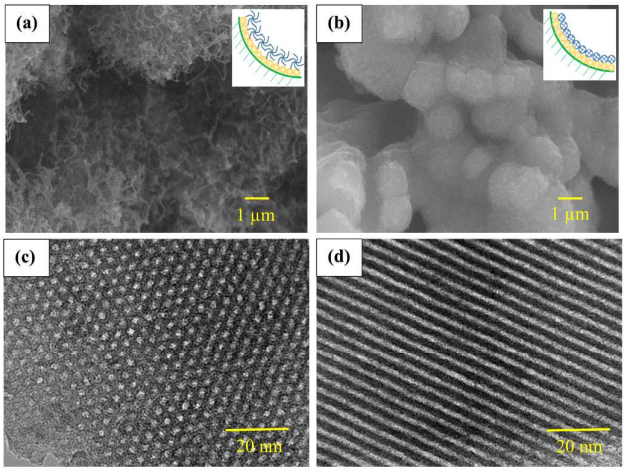

Fig. 10 The SEM images for bilayer carbon coating cathodes with (a) top-layer of carbon nanofiber and (b) top-layer of mesoporous carbon before cell test. Schematic diagram illustrates the bilayer structure for carbon over LATP surface. Arc (at bottom) represents the wall for a pore inside porous cathode, ball (in middle) represents carbon nanoparticles, and curve (on surface) in (a) represents carbon nanofiber, and the porous ball (on surface) in (b) represents mesoporous carbon. TEM images for prepared mesoporous carbon, the surface in (c) is perpendicular to that in (d).

Cycle performances and high-rate discharge properties

To evaluate the cycle performance, the novel Li-O_2 battery was cycled with a fixed capacity of 1,000 mA h g^{-1}_{carbon} or 5,000 mA h g^{-1}_{carbon} at a constant current density of 0.15 mA cm^{-2}, as shown in Fig. 8a and c. The capacity retention on cycling is shown in Fig. 8b and d where it is seen that 100% of the initial capacity is retained after 100 or 20 cycles, showing an outstanding cycling stability. The two similar batteries have different discharge depths but the same cycle time. When cycling at a fixed capacity of 1,000 mA h $g^{-1}_{carbon,}$ the energy efficiency with cycling decreased from 68% to 62%, with the voltage plateau of discharge was decreased from 2.62 to 2.47 V while the voltage plateau of charge was increased from 3.82 to 4.01 V. When cycling at a fixed capacity of 5,000 mA h $g^{-1}_{carbon,}$ the energy efficiency with cycling decreased from 64% to 58%, with the voltage plateau of discharge was decreased from 2.59 to 2.44 V while the voltage plateau of charge was increased from 4.05 to 4.18 V.

Fig. 9a shows galvanostatic discharge curves for the novel Li-O_2 battery at different current densities. The open circuit voltages (OCVs) were all close to 3.4 V, and the discharge capacity was decreased from 16,800 to 12,000 mA h g^{-1}_{carbon} when increasing current density from 0.1 to 0.3 mA cm^{-2}. When

further increasing the current density, the discharge plateau disappeared. To achieve a much better rate of performance, carbon loading was further increased from 2 to 3 mg cm^{-2}. As a result, the highest discharge current density was improved to 2.5 mA cm^{-2} as given in Fig. 9b. Please note that the local current density decreases from the interface between the electrolyte and cathode layers toward the end of the cathode, as demonstrated by the gradient distribution of the discharge product shown in Fig. S3. Even with a decrease in the discharge capacity-density, the increase in carbon loading leads to a significant performance boost. However, the increase for carbon loading should be limited by the fact that there is always a balance between electron transport and oxygen diffusion in the monolayer carbon coated cathode. As shown in Fig. 2d, the carbon coating shows less porosity, suggesting that if the thickness were to be further increased, the diffusion of gaseous oxygen in the direction perpendicular to the layer surface must be inhibited. To remedy this situation, a bilayer carbon coating with porous top-layer and relative dense bottom-layer was proposed and appeared to resolve the issue. Two techniques were used to introduce the porous carbon top-layer, including chemical vapour deposition (CVD) and ultrasonic assisted impregnation. Fig. 10a and b display the interior surfaces of two kinds of bilayer carbon coated porous cathode; (a) the first with carbon nanofibers network as the top-layer and nanoparticles as the bottom-layer and (b) the second with mesoporous carbon as the top-layer and nanoparticles as the bottom-layer. The mesoporous structure was characterized by a transmission electron microscopy (TEM). Tunnels of 5 nm in diameter ranked neatly in Fig. 10c and d. After introducing an additional top-layer carbon, the discharge current densities for the Li-O_2 batteries were improved to the highest value of 13 mA cm^{-2} with an apparent discharge plateau above 2.0 V, as shown in Fig. 9c. In comparison, the discharge curve for monolayer carbon coated Li-O_2 battery was also given without an obvious discharge plateau at 13 mA cm^{-2}. However, the capacities were reduced to <2,000 mA h g^{-1}_{carbon}, which should be attributed to that the fact that the top-layer of carbon is relatively inert for electrochemical reactions. Additionally, the top-layer is relatively far away from LATP-backbone surface leading to a longer Li^+ transmission path. The mesoporous carbon based battery exhibited a relatively higher capacity density of 1,600 mA h g^{-1}_{carbon}, 2 times higher than that of the carbon-fiber based battery. Our group is currently embarking on a series of studies to demonstrate the performances and mechanisms for the novel Li-O_2 battery with a bilayer carbon coated cathode.

Conclusions

In conclusion, a Li-O_2 battery with an integrated cathode with electrolyte was proposed and fabricated for the first time. In the novel battery, the thickness of LATP solid-state electrolyte layer was decreased from 600 μm to 36 μm, the porosity of the solid-state cathode was increased to 78%, and the TPBs were expanded from the conventional electrolyte/cathode interface to the entire solid-state cathode without the aid of liquid electrolytes. In the integrated cathode, the LATP scaffold provides rich Li^+ transport pathways, while a carbon coating over LATP surface prepared through an impregnation process provides electron transport pathways and at the same time serves as catalyst for ORR and OER processes. A Li-O_2 battery based on this novel integrated structure delivered a rechargeable capacity of 16,800 mA h g^{-1}_{carbon} at the first circle and 0.1 mA cm^{-2}. XRD results confirmed that LATP is stable enough for the Li-O_2 battery operation under the testing conditions. FTIR results demonstrated the formation and decomposition of product Li_2O_2. The change in the product morphology during discharge and charge were visually displayed by SEM. A mechanism based on low-level conductivity of Li_2O_2 was proposed to explain the product formation inside the novel solid-state cathode. The present battery was able to sustain 100 cycles at a ~6% depth of discharge (DOD) of 1,000 mA h g^{-1}_{carbon}, with an energy efficiency of 62%. It was also able to sustain 20 cycles at a ~30% DOD of 5,000 mA h g^{-1}_{carbon}, with an energy efficiency of 58%. The current density of discharge can be increased to 2.5 mA cm^{-2} by increasing carbon loading, and it can be further increased to the highest value of 13 mA cm^{-2} by introducing another porous top-layer (with carbon nanofiber or mesoporous carbon) to form a bilayer carbon coating. Further development and evaluation for the bilayer carbon coating cathode is under development in our group. This battery design can solve two major problems of solid-state Li-O_2 batteries, namely, high ohmic loss and limited active interface, with high potential applications.

Acknowledgements

The work described in this paper was fully supported by a grant from the Research Grants Council of the Hong Kong Special Administrative Region, China (Project No. 16213414).

Notes and references

1. P. G. Bruce, S. A. Freunberger, L. J. Hardwick and J. M. Tarascon, *Nat. Mater.*, 2012, **11**, 19-29.
2. Y. Sun, *Nano Energy*, 2013, **2**, 801-816.
3. T. Zhang and H. Zhou, *Nat. Commun.*, 2013, **4**, 1817-1823.
4. P. Tan, Z. H. Wei, W. Shyy and T. S. Zhao, *J. Power Sources*, 2013, **109**, 275-282.
5. Y.-C. Lu, E. J. Crumlin, G. M. Veith, J. R. Harding, E. Mutoro, L. Baggetto, N. J. Dudney, Z. Liu and Y. Shao-Horn, *Sci. Rep.*, 2012, **2**, 715-720.
6. M. A. Rahman, X. Wang and C. Wen, *J. Appl. Electrochem.*, 2014, **44**, 5-22.
7. Y. Shao, F. Ding, J. Xiao, J. Zhang, W. Xu, S. Park, J.-G. Zhang, Y. Wang and J. Liu, *Adv. Funct. Mater.*, 2013, **23**, 987-1004.
8. B. Key, D. J. Schroeder, B. J. Ingram and J. T. Vaughey, *Chem. Mater.*, 2012, **24**, 287-293.
9. P. Kichambare, S. Rodrigues and J. Kumar, *ACS Appl. Mater. Inter.*, 2011, **4**, 49-52.
10. M. Balaish, A. Kraytsberg and Y. Ein-Eli, *Phys. Chem. Chem. Phys.*, 2014, **16**, 2801-2822.
11. K. Hoshina, K. Yoshima, M. Kotobuki and K. Kanamura, *Solid State Ionics*, 2012, **209-210**, 30-35.

12. H. Nakano, K. Dokko, M. Hara, Y. Isshiki and K. Kanamura, *Ionics*, 2007, **14**, 173-177.
13. K. Nagata and T. Nanno, *J. Power Sources*, 2007, **174**, 832-837.
14. T. Zhang, N. Imanishi, Y. Shimonishi, A. Hirano, Y. Takeda, O. Yamamoto and N. Sammes, *Chem. Commun.*, 2010, **46**, 1661-1663.
15. Y. Lu, J. B. Goodenough and Y. Kim, *J. Am. Chem. Soc.*, 2011, **133**, 5756-5759.
16. A. Manthiram and L. Li, *Adv. Energy Mater.*, 2015, **5**.
17. Y. Wang and H. Zhou, *Energy Environ. Sci.*, 2011, **4**, 1704-1707.
18. H. Kitaura and H. Zhou, *Adv. Energy Mater.*, 2012, **2**, 889-894.
19. Y. Shen, D. Sun, L. Yu, W. Zhang, Y. Shang, H. Tang, J. Wu, A. Cao and Y. Huang, *Carbon*, 2013, **62**, 288-295.
20. Z. Wen, C. Shen and Y. Lu, *ChemPlusChem*, 2015.
21. M. Kotobuki, Y. Isshiki, H. Munakata and K. Kanamura, *Electrochim. Acta*, 2010, **55**, 6892-6896.
22. X. Wang, D. Zhu, M. Song, S. Cai, L. Zhang and Y. Chen, *ACS Appl. Mater. Inter.*, 2014, **6**, 11204-11210.
23. H. G. Jung, J. Hassoun, J. B. Park, Y. K. Sun and B. Scrosati, *Nat. Chem.*, 2012, **4**, 579-585.
24. G. Girishkumar, B. McCloskey, A. Luntz, S. Swanson and W. Wilcke, *J. Phys. Chem. Lett.*, 2010, **1**, 2193-2203.
25. R. Padbury and X. Zhang, *J. Power Sources*, 2011, **196**, 4436-4444.
26. S. D. Jackman and R. A. Cutler, *J. Power Sources*, 2012, **218**, 65-72.
27. P. Hartmann, T. Leichtweiss, M. R. Busche, M. Schneider, M. Reich, J. Sann, P. Adelhelm and J. Janek, *J. Phys. Chem. C*, 2013, **117**, 21064-21074.
28. H. Buschmann, S. Berendts, B. Mogwitz and J. Janek, *J. Power Sources*, 2012, **206**, 236-244.
29. J. Christensen, P. Albertus, R. S. Sanchez-Carrera, T. Lohmann, B. Kozinsky, R. Liedtke, J. Ahmed and A. Kojic, *J. Electrochem. Soc.*, 2011, **159**, R1-R30.
30. J. Xiao, D. Mei, X. Li, W. Xu, D. Wang, G. L. Graff, W. D. Bennett, Z. Nie, L. V. Saraf, I. A. Aksay, J. Liu and J. G. Zhang, *Nano Lett.*, 2011, **11**, 5071-5078.
31. N. Akhtar and W. Akhtar, *Int. J. Energ. Res.*, 2015, **39**, 303-316.
32. V. Aravindan, W. Chuiling and S. Madhavi, *RSC Adv.*, 2012, **2**, 7534-7539.
33. N. Arun, V. Aravindan, W. C. Ling and S. Madhavi, *J. Alloy. Compd.*, 2014, **603**, 48-51.
34. V. Aravindan, M. Ulaganathan, W. C. Ling and S. Madhavi, *ChemElectroChem*, 2015, **2**, 231-235.
35. C. Xia, M. Waletzko, L. Chen, K. Peppler, P. J. Klar and J. R. Janek, *ACS Appl. Mater. Inter.*, 2014, **6**, 12083-12092.
36. J. Lu, L. Li, J. B. Park, Y. K. Sun, F. Wu and K. Amine, *Chem. Rev.*, 2014, **114**, 5611-5640.
37. L. Zhong, R. R. Mitchell, Y. Liu, B. M. Gallant, C. V. Thompson, J. Y. Huang, S. X. Mao and Y. Shao-Horn, *Nano Lett.*, 2013, **13**, 2209-2214.
38. D. Zhai, H.-H. Wang, K. C. Lau, J. Gao, P. C. Redfern, F. Kang, B. Li, E. Indacochea, U. Das, H.-H. Sun, H.-J. Sun, K. Amine and L. A. Curtiss, *J. Phys. Chem. Lett.*, 2014, **5**, 2705-2710.
39. Z. Peng, S. A. Freunberger, Y. Chen and P. G. Bruce, *Science*, 2012, **337**, 563-566.
40. F. Li, T. Zhang and H. Zhou, *Energy Environ. Sci.*, 2013, **6**, 1125-1141.
41. R. Black, B. Adams and L. F. Nazar, *Adv. Energy Mater.*, 2012, **2**, 801-815.
42. M. D. Bhatt, H. Geaney, M. Nolan and C. O'Dwyer, *Phys. Chem. Chem. Phys.*, 2014, **16**, 12093-12130.
43. A. C. Luntz and B. D. McCloskey, *Chem. Rev.*, 2014, **114**, 11721-11750.
44. E. Quartarone and P. Mustarelli, *Chem. Soc. Rev.*, 2011, **40**, 2525-2540.
45. J.-S. Lee, S. Tai Kim, R. Cao, N.-S. Choi, M. Liu, K. T. Lee and J. Cho, *Adv. Energy Mater.*, 2011, **1**, 34-50.
46. L. Johnson, C. Li, Z. Liu, Y. Chen, S. A. Freunberger, J.-M. Tarascon, P. C. Ashok, B. B. Praveen, K. Dholakia and P. G. Bruce, *Nat. Chem.*, 2014, **6**, 1091-1099.
47. B. D. Adams, C. Radtke, R. Black, M. L. Trudeau, K. Zaghib and L. F. Nazar, *Energy Environ. Sci.*, 2013, 6, 1772-1778.
48. Y.-C. Lu, B. M. Gallant, D. G. Kwabi, J. R. Harding, R. R. Mitchell, M. S. Whittingham and Y. Shao-Horn, *Energy Environ. Sci.*, 2013, **6**, 750-768.
49. V. Viswanathan, K. S. Thygesen, J. Hummelshøj, J. K. Nørskov, G. Girishkumar, B. McCloskey and A. Luntz, *J. Chem. Phys.*, 2011, **135**, 214704(1-10).
50. M. D. Radin, J. F. Rodriguez, F. Tian and D. J. Siegel, *J. Am. Chem. Soc.*, 2011, **134**, 1093-1103.
51. M. D. Radin and D. J. Siegel, *Energy Environ. Sci.*, 2013, **6**, 2370-2379.
52. H. Zheng, D. Xiao, X. Li, Y. Liu, Y. Wu, J. Wang, K. Jiang, C. Chen, L. Gu, X. Wei, Y. S. Hu, Q. Chen and H. Li, *Nano Lett.*, 2014, **14**, 4245-4249.

The world's energy demands have been steadily increasing over the years, with a widening gap between demand and supply, particularly in emerging industries such as electric vehicles. The switch from fossil-fuelled transportation to electric cars is undoubtedly the trend of the future, helping to relieve climate change and securing energy sustainability. Development in this area, however, has slowed down considerably due to a lack of satisfactory electrical energy-storage systems. A promising candidate is the lithium-air battery, possessing the advantages of being a portable power source and exhibiting the highest theoretical specific energy density among known metal-based electrochemical batteries. However, the inherent lithium-air battery is also double-edged to several critical challenges in operation. To address these problems, a solid-state lithium-air battery system has been developed with the introduction of solid-state Li-ion conductors. However, a high internal resistance and limited triple-phase boundaries are two critical issues that limit the performance of conventional solid-state lithium-air batteries. In this work, we propose and fabricate a novel solid-state lithium-air battery with an integrated electrolyte and cathode structure. This design allows a thin electrolyte layer and a highly porous cathode, both of which contribute to a significant reduction in the internal resistance, while increasing triple-phase boundaries.